

AD-A227 342

DTIC FILE COPY

(2)

GL-TR-90-0091

ENVIRONMENTAL RESEARCH PAPERS, NO. 1061

Mesoscale Features of a Winter Storm:
Dual Doppler Velocity Fields and
Differential Reflectivity

JAMES I. METCALF
FRANK H. RUGGIERO

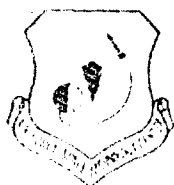


10 April 1990

DTIC
ELECTE
OCT. 10 1990
S B D

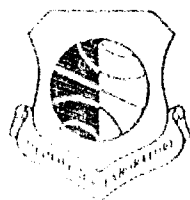


Approved for public release; distribution unlimited.



*Original contains color
plates: All DTIC reproductions
will be in black and
white*

**BEST
AVAILABLE COPY**



ATMOSPHERIC SCIENCES DIVISION

PROJECT 7670

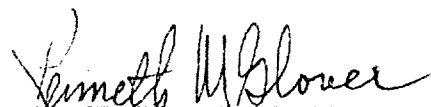
GEOPHYSICS LABORATORY

HANSCOM AFB, MA 01731-5000

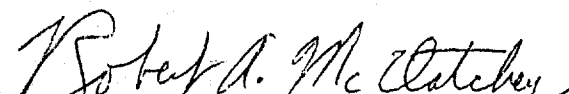
90 10 09 123

"This technical report has been reviewed and is approved for publication"

FOR THE COMMANDER



KENNETH M. GLOVER, Chief
Ground Based Remote Sensing Branch
Atmospheric Sciences Division



ROBERT A. MCCLATCHEY, Director
Atmospheric Sciences Division

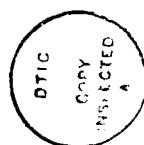
This report has been reviewed by the ESD Public Affairs Office (PA) and is releasable to the National Technical Information Service (NTIS).

Qualified requestors may obtain additional copies from the Defense Technical Information Center. All others should apply to the National Technical Information Service.

If your address has changed, or if you wish to be removed from the mailing list, or if the addressee is no longer employed by your organization, please notify GL/IMA, Hanscom AFB, MA 01731. This will assist us in maintaining a current mailing list.

Preface

The observations and analysis presented in this report represent the first joint use of the radars of the Geophysics Laboratory (GL) and the Massachusetts Institute of Technology (MIT) for synthesis of wind fields. Operation of the MIT radar was supported by GL through Contract No. F19628-87-M-0004, with Prof. Earle Williams as Principal Investigator. We are grateful to Prof. Williams for his collaboration in the acquisition of the data and his review of this report. We are also grateful to Mr. Ralph Donaldson of ST Systems Corp. for his insight on the interpretation of the Doppler velocity observations, to Dr. H. Stuart Muench of GL for his assistance in understanding the synoptic and mesoscale aspects of the analysis, and to Dr. F. Ian Harris of ST Systems Corp. for his assistance in the use of CEDRIC, the Doppler radar data analysis software package.



Accession For	
NTIS GRA&I	<input checked="checked" type="checkbox"/>
DTIC TAB	<input type="checkbox"/>
Unannounced	<input type="checkbox"/>
Justification	
By _____	
Distribution/	
Availability Codes	
Dist	Avail and/or Special
A-1	

Contents

1. INTRODUCTION	1
2. SYNOPTIC CONDITIONS	2
3. RADAR MEASUREMENTS	8
4. ANALYSIS OF RADAR OBSERVATIONS	9
4.1. Thermodynamic Phase of Precipitation	9
4.2. Mesoscale Wind Perturbations Aloft	15
4.3. Surface Weather Events	28
5. SUMMARY	31
REFERENCES	33

Illustrations

1. Analysis of 850-mb Pressure Surface at 1200 UT	3
2. Map of Southeastern New England	4
3. Sounding from Chatham, Mass., at 1200 UT	6
4. Sounding from Portland, Maine, at 1200 UT	7
5. Absolute and Differential Reflectivity at 0909 EST	11
6. Absolute and Differential Reflectivity at 1021 EST	12
7. Absolute Reflectivity at 1112 EST	13
8. Vertical Section of Absolute and Differential Reflectivity at 0956 EST	14
9. Absolute and Differential Reflectivity at 1219 EST	16
10. Doppler Mean Velocity in Azimuthal Scan at 1101 EST	19
11. Doppler Mean Velocity in Azimuthal Scans at 1316 EST	20
12. Synthesized Velocity Fields at 1314 and 1401 EST	21
13. Profiles of Mean Horizontal Wind in Analysis Grid	22
14. Horizontal Divergence at 2 km Height	24
15. Vertical Vorticity at 2 km Height	26
16. Absolute Reflectivity and Doppler Mean Velocity in Azimuthal Scans at 1419 EST	30

Mesoscale Features of a Winter Storm: Dual-Doppler Velocity Fields and Differential Reflectivity

1. INTRODUCTION

The 11-cm wavelength (S-band) Doppler radar operated by the Geophysics Laboratory (GL) in Sudbury, Mass., has been used for several years for investigations of the physics and kinematics of storms, including both convective storms, typical of the late spring and summer, and synoptic scale low-pressure systems, typical of the fall and winter. This radar was modified in 1985 and 1986 to permit the measurement of the linear polarization differential reflectivity (Z_{DR}) for investigations of the microphysics of clouds and precipitation.^{1, 2} One of our goals has been to integrate the microphysical information with two- and three-dimensional vector wind fields for more comprehensive understanding of the

(Received for publication 6 April 1990)

(The list of references begins on page 33)

development of precipitation systems. The wind fields can be derived from coordinated observations by the GL radar and the 11-cm wavelength Doppler radar at the Massachusetts Institute of Technology (MIT) in Cambridge, Mass. Several storms were observed by both radars during the period January–March 1988. This report describes small-scale features of the cyclonic storm of 12 February 1988. This storm is of interest because of the changing types of precipitation that it generated and because of certain features observed in the Doppler velocity displays. In particular, the Doppler velocity data from the GL radar suggest the presence of a mesoscale vortex that persisted for about 2½ hr. A preliminary analysis³ showed a possible relationship between this feature and a mesoscale trough and led to the hypothesis that the velocity feature was associated with the development of a coastal front. This report presents the results of our further investigation of the precipitation microphysics and the mesoscale velocity field of the storm.

2. SYNOPTIC CONDITIONS

Between 1900 EST on 11 February 1988 and 0700 EST on 12 February 1988 (0000 and 1200 UT on 12 February) a slowly moving, intensifying, cutoff low was located over upper Michigan and Lake Huron. The 850 mb analysis at 0700 EST (1200 UT) on 12 February (Figure 1) shows the 850 mb low center over the Bruce Peninsula, on the east side of Lake Huron. There is some evidence of a low-level southerly jet in the southeast quadrant of the circulation around the low center. The highest wind speeds in the vicinity of the 850 mb low were over Atlantic City, N. J.; Wallops Island, Va.; and Greensboro, N. C. The surface low pressure center associated with the upper level circulation was located in the vicinity of Lakes Erie and Huron; a secondary area of low pressure was developing off the coast of New Jersey. This area of developing low pressure intensified and moved to the east-northeast, remaining south of New England, during the daylight hours of 12 February (Figure 2). At 1600 EST (2100 UT) it was located about 100 km south of the coast at the border of Rhode Island and Massachusetts, or about 200 km south of the GL radar, and was deepening at a rate of about 1 mb hr⁻¹. A warm front extending eastward

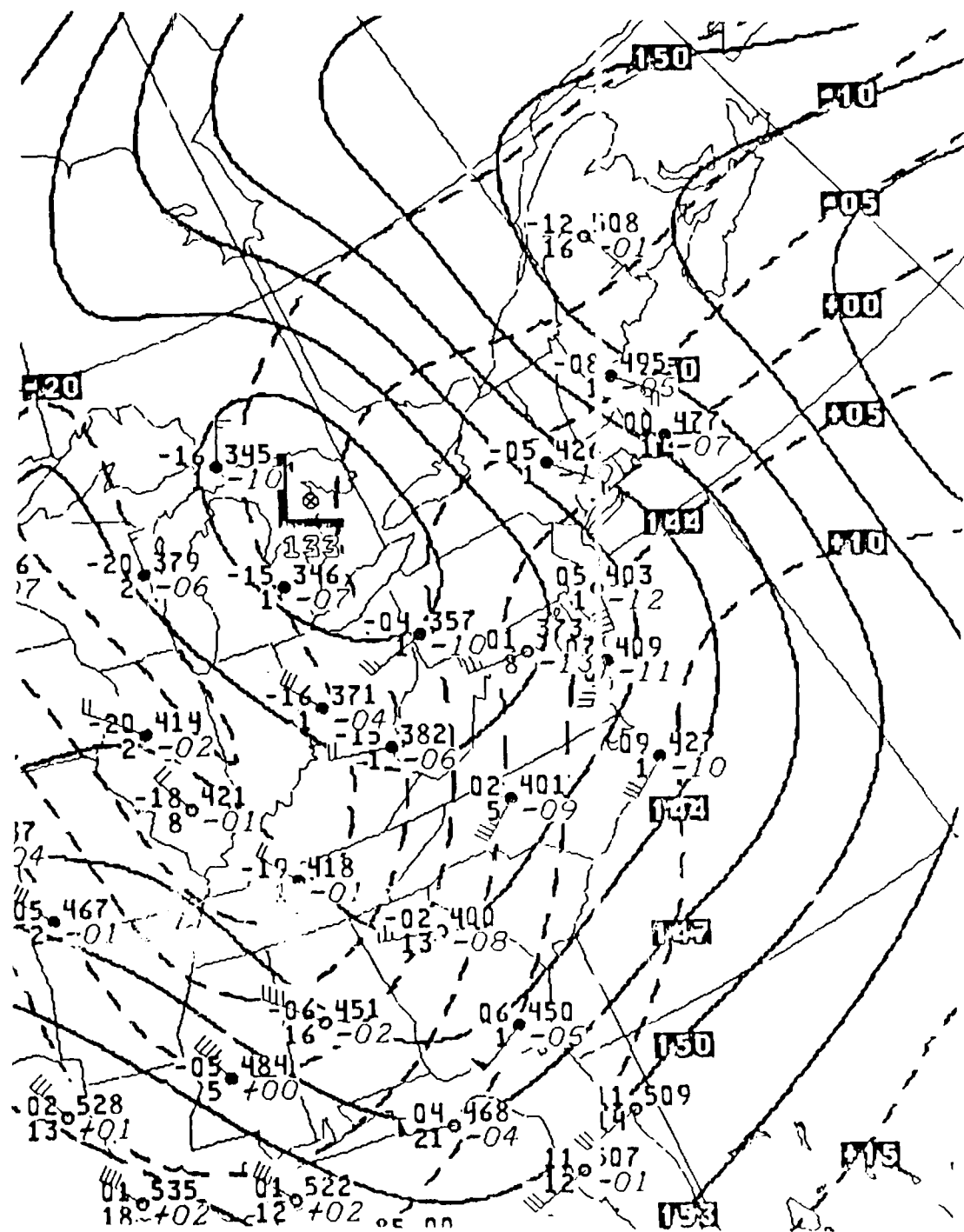


Figure 1. Analysis of 850-mb Pressure Surface at 1200 UT. Analysis shows cutoff low over Great Lakes and southerly flow over southern New England.

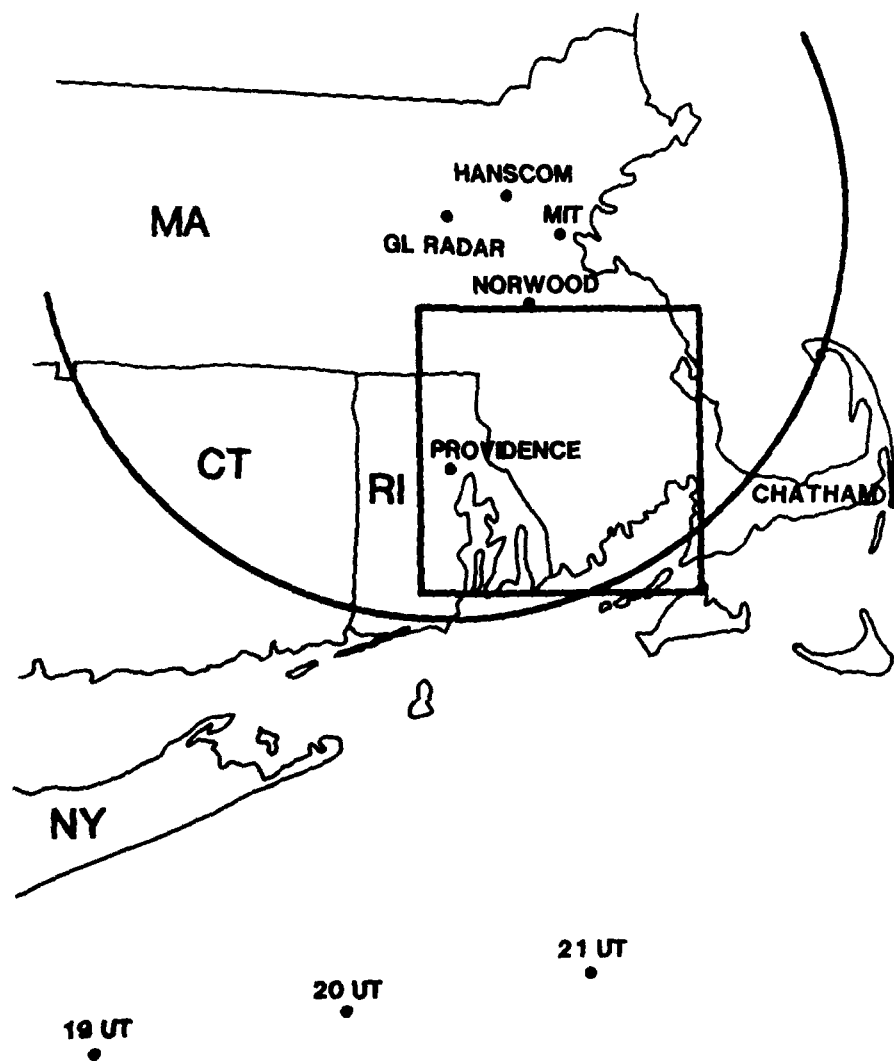


Figure 2. Map of Southeastern New England. Map is annotated to show locations of radars and reporting stations mentioned in text, location of the analysis grid, and locations of the surface low pressure center at 1900, 2000, and 2100 UT (1400, 1500, and 1600 EST) interpolated from sea-level analyses at 1800 and 2100 UT. Circular arc denotes 115 km range from the Geophysics Laboratory radar.

at the surface from the low pressure center was evident in soundings at 0700 EST (1200 UT) from both Chatham, Mass. (Figure 3), and Portland, Maine (Figure 4). The wind was easterly through the lowest kilometer and veered to southerly at 2 km; similar characteristics were evident in the Doppler radar data throughout the morning and early afternoon. The sounding from Chatham revealed that the temperature was above 0°C as high as 805 mb (about 2 km height) but was within less than two degrees of 0°C throughout the lowest 2 km. This thermal structure bears some similarity to the deep 0°C isothermal layers in stratiform precipitation described by Stewart⁴ and by Szeto et al.⁵

Precipitation spread northward over New England ahead of the surface position of the front, beginning as snow in all but the south coastal areas. The change to rain progressed northward, accompanying the northward advection of warmer air in the lowest few kilometers. Precipitation at the GL radar site began as snow about 0400 EST, mixed with rain shortly after 1200 EST, and ended about 1400 EST. The precipitation was initially stratiform in structure, but became more showery as clearing progressed from the west. Clearing of the heaviest rain (greater than 0.1 inch hr^{-1}) occurred over southern New England between 1100 and 1600 EST, but precipitation continued intermittently over much of this area until the early hours of 13 February.

A typical feature of coastal cyclonic storms such as this one is the formation of a low-level front, known as a coastal front,⁶ as warm air approaching from the east or southeast overruns cold air near the ground, creating a strong temperature gradient near the coastline or as much as 50 km inland. The hourly temperature data from 12 February 1988 suggest the formation of a coastal front across southern Rhode Island by 1000 EST. Some of the temperature differences at the surface suggest horizontal gradients as high as 0.2 K km^{-1} , typical of the coastal fronts described by Bosart et al.,⁶ but the spatial continuity of these gradients was limited and the surface winds in that area did not exhibit cyclonic curvature or convergence typical of coastal fronts. The surface winds were generally easterly or east-northeasterly all along the coast and 100 km or more inland. Thus, contrary to the preliminary suggestion that the observed features were associated with a coastal front, we now conclude that these features were the result of other mechanisms. Substantial advection of warm air at

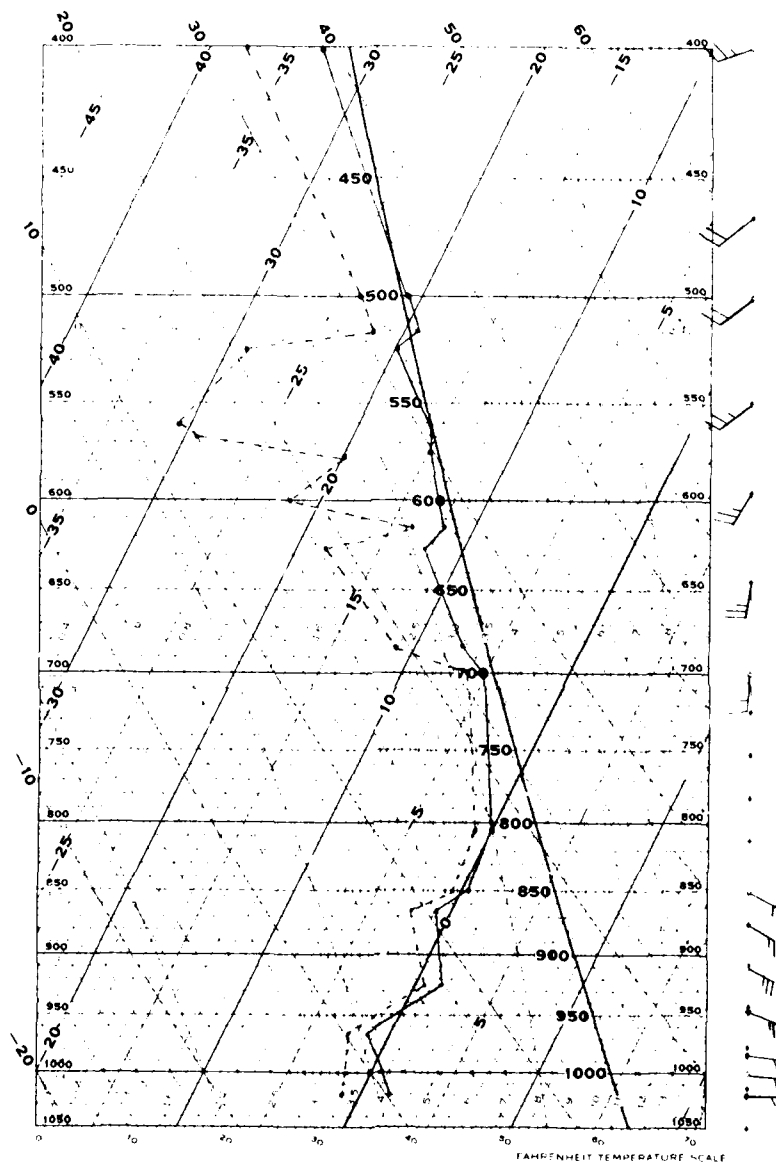


Figure 3. Sounding from Chatham, Mass., at 1200 UT. Temperature and dew point are plotted on a modified Skew T, log p diagram. Wind vectors are plotted with conventional notation. Flow is east-northeasterly at surface and veers to southerly at 2 km height.

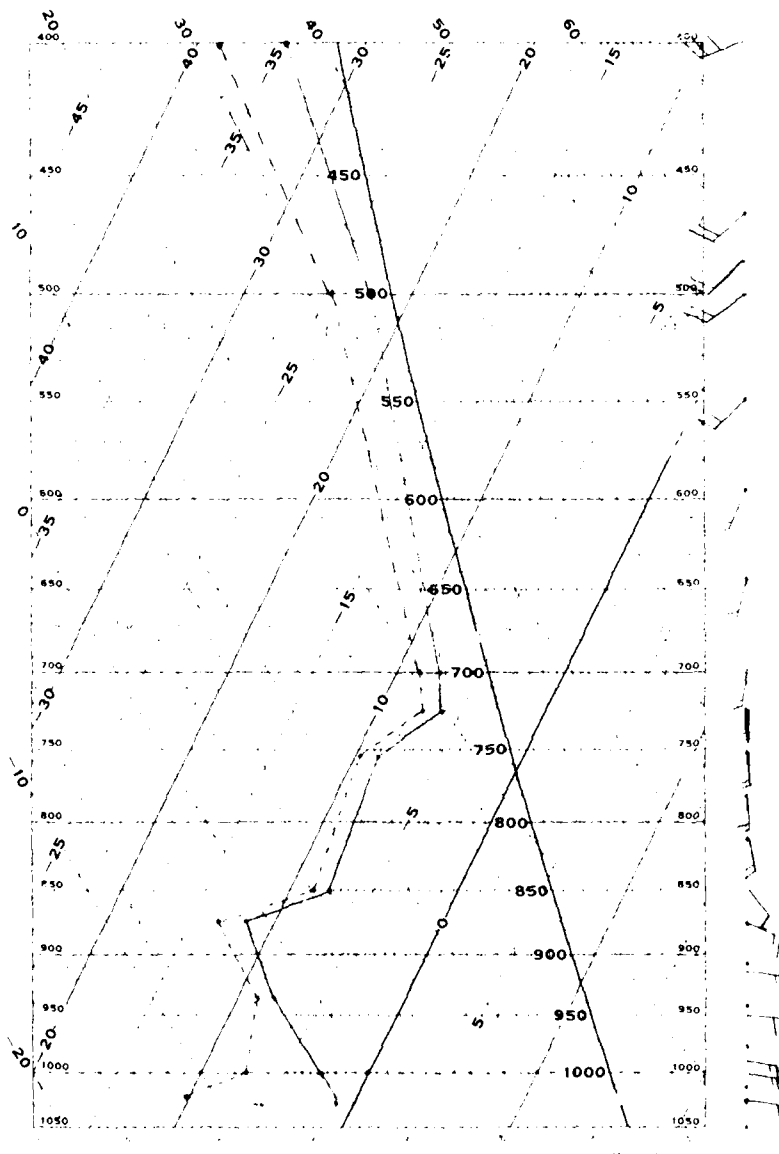


Figure 4. Sounding from Portland, Maine, at 1200 UT. Format is identical to that of Figure 3.

low levels over most of southeast New England led to strong static stability in the lowest 2 km. This stability, together with the deepening and eastward movement of the low pressure center to the south, provided the setting for the mesoscale wind variations observed by radar during the late morning and early afternoon.

3. RADAR MEASUREMENTS

The GL radar, located about 35 km (22 miles) west of Boston, Mass., was operated with a pulse repetition frequency of 1000 Hz, which yielded an unambiguous range of 150 km and an unambiguous Doppler velocity interval of $\pm 27.65 \text{ m sec}^{-1}$. It was operated generally in a volume scanning mode from 1830 EST on 11 February to 1535 EST on 12 February. Azimuthal scans were made at elevation angles of 0.5, 1.5, 2.5, 3.5, and 4.5°. A network of three switchable circulators in the microwave circuit alternated the polarization of successive transmitted pulses between horizontal and vertical. The data archive comprises the absolute reflectivity (Z), the differential reflectivity (Z_{DR}), and the Doppler mean velocity in 768 gates at 150-m increments in range, to a maximum range of 115 km, averaged and sampled at intervals of 0.128 sec (approximately 0.93° resolution in azimuthal scans). The linear polarization differential reflectivity is defined by

$$Z_{DR} = Z_H / Z_V,$$

or by the logarithmic equivalent, where Z_H and Z_V denote the reflectivity factor measured with horizontal and vertical polarization, respectively.⁷ Its use in the discrimination of solid and liquid hydrometeors is well documented in the meteorological literature.⁸

The MIT radar, located 33 km from the GL radar on an azimuth of 100°, was operated with a pulse repetition frequency of 721 Hz, which yielded an unambiguous range of 208 km and an unambiguous Doppler velocity interval of $\pm 20.0 \text{ m sec}^{-1}$. It was operated from 2350 EST on 11 February until 0550 EST on 13 February, also predominantly in a volume-scanning mode. Until about 1200 EST on 12 February only two elevation angles (0.7 and 1.5°) were used; subsequently, volume scans comprising five elevation angles (0.7, 1.5, 2.2, 3.0, and 4.0°) were made at intervals of about 10

minutes. The data archive comprises absolute reflectivity, Doppler mean velocity, and Doppler spectrum variance sampled in 200 gates, spaced by 0.25 km from 0–10 km range and by 1 km from 11–170 km range, with azimuthal resolution of 0.7–0.9°. The data selected for detailed velocity analysis were acquired between 1214 and 1405 EST on 12 February.

4. ANALYSIS OF RADAR OBSERVATIONS

4.1. Thermodynamic Phase of Precipitation

The storm of 12 February 1988 was typical of coastal winter storms in that precipitation began as snow except along the southern coast and changed to rain progressively as warmer air was advected northward. Displays of the differential reflectivity at low altitude revealed values near unity (0 dB), indicative of the ice phase, initially covering most of eastern Massachusetts and northern Connecticut and Rhode Island. An apparent transition line, to the south of which the differential reflectivity was greater than unity (positive decibel values), moved northward during the morning hours. It was located about 60 km south-southeast of the GL radar at 0909 EST (Figure 5) and advanced to 40 km range by 1021 EST (Figure 6) and 35 km at 1050 EST. Thereafter it became less well defined, as the precipitation structure developed more spatial variability. Precipitation in Providence, R. I., about 70 km south of the radar, was reported as ice pellets (sleet) at 0700 EST; this indicates that rain, which typically yields a positive differential reflectivity, was present aloft. The nearest reporting station north of Providence is Norwood, Mass., where snow continued until after 1100 EST. By that time, the heaviest precipitation was concentrated in a band lying between 45 and 100 km southeast of the GL radar and extending southward and east-northeastward on the radar display (Figure 7). The differential reflectivity was positive at low altitudes in most of this band, except for a region of near 0 dB toward the eastern end. The change from snow to rain at the radar site occurred as this band of precipitation slowly expanded toward the northwest.

In the interpretation of azimuthal radar scans through stratiform precipitation, one must take care to separate features due to horizontal

variations from features due to vertical variations, particularly near the melting level. In the present case we attempted to do this by performing a series of elevation scans at several azimuths about 1000 EST and about 1300 EST. The resulting vertical cross-section at 0956 EST, nearly perpendicular to the line of transition of differential reflectivity, is shown in Figure 8. The vertical structure reveals a maximum of absolute reflectivity near 2–3 km height spanning much of the surveillance range. This feature and the increased differential reflectivity below 3 km height beyond about 50 km range are consistent with the presence of melting precipitation, that is, a "bright band." At 1000 EST the temperature was 1.1°C in Providence, R. I., about 70 km south of the radar. While this temperature suggests a very low melting level (about 200 m, based on a moist adiabatic lapse rate), we should recall that the morning sounding from Chatham showed temperatures not far from 0°C to a height of 2 km, where we might therefore expect to see the bright band. The radar observation, which shows positive decibel values of differential reflectivity and relatively high values of absolute reflectivity up to 2 km, suggests that melting begins at this height. Two factors may contribute to the large vertical extent of the apparent bright band. First, because the temperature is nearly isothermal in the lowest 2 km, the melting may not proceed fast enough to yield a well defined bright band. Second, the vertical dimension of the radar beam at these ranges (1.2 km at 70 km range) may be too great to reveal details of the melting level. The enhanced absolute reflectivity at ranges of 15–50 km is unlikely to represent a melting level, because there is no corresponding enhancement of differential reflectivity.

In contrast to the structure revealed in Figure 8, azimuthal scans about 1150 EST showed structure suggestive of a bright band in the southeast sector near 1.5 km height (at ranges of 20–35 km). The change of precipitation from snow to rain in Norwood, Mass. (36 km on 133° azimuth from the GL radar), occurred between 1100 and 1200 EST. The rapidly

Scale of *absolute reflectivity* in Figures 5–9 and Figure 16 runs from -28 to $+47$ dBZ. Numbers shown in blue denote negative values. For example, gray shading denotes 17–22 dBZ; yellow, 22–27 dBZ; black, 27–32 dBZ; and red, 32–37 dBZ. *Differential reflectivity* runs from -12.8 to $+12.8$ dB on a numerical scale of 0 to 100, or about 4 counts per decibel. Thus green denotes -1 ± 0.5 dB; gray, 0 ± 0.5 dB; yellow, 1 ± 0.5 dB; and red, 2 ± 0.5 dB.

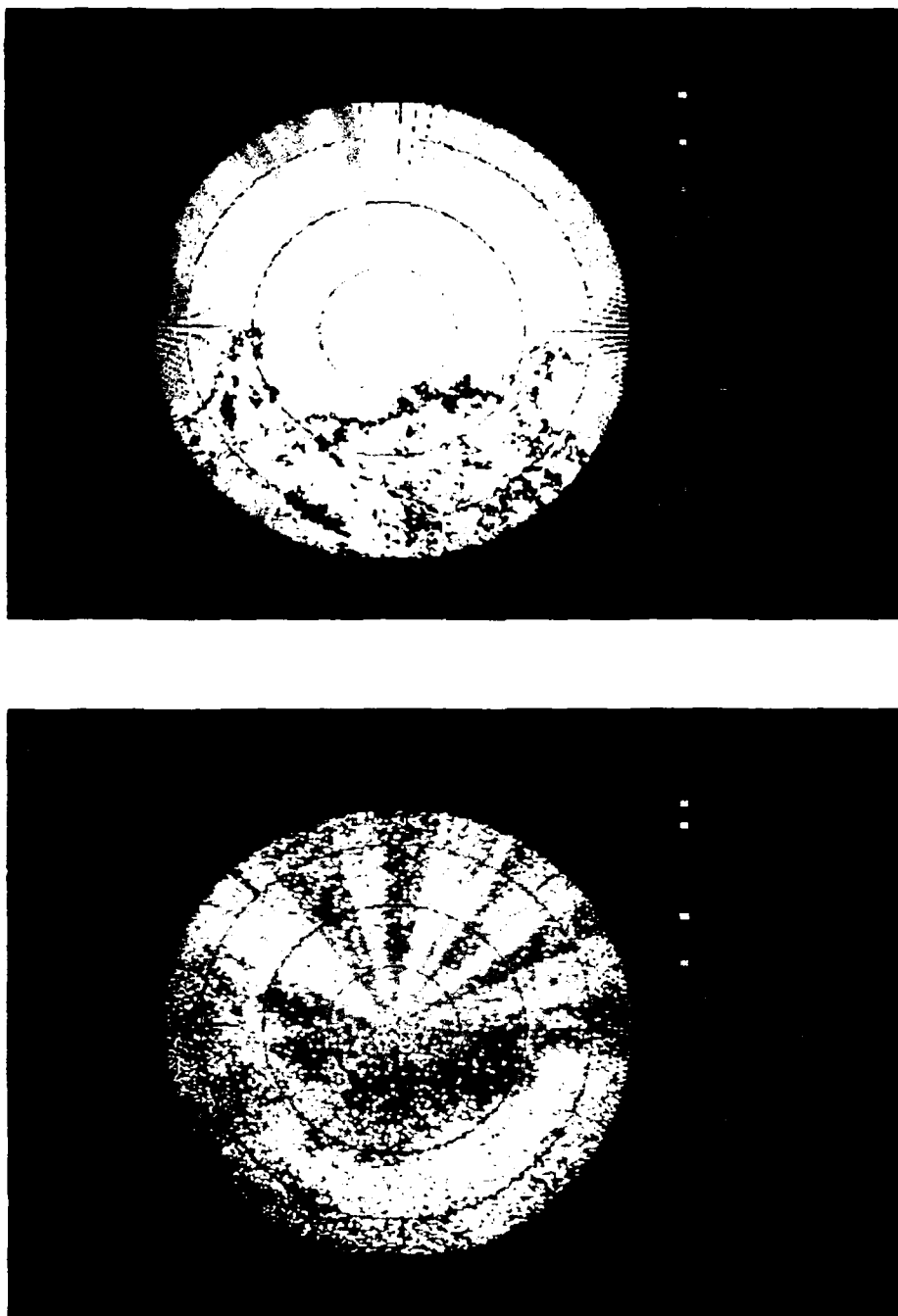


Figure 5. Absolute and Differential Reflectivity at 0909 EST. Range is marked at increments of 32 km and maximum range is 115 km. Color scales are described in footnote on Page 10. *Upper panel:* Azimuthal scan at 0.5° elevation angle shows highest absolute reflectivity beyond 40 km south of the GL radar and relatively uniform values in the northern part of the display. *Lower panel:* Differential reflectivity is most strongly positive (yellow denotes 1 ± 0.5 dB) beyond about 60 km south of the radar and near zero (gray) or only weakly positive elsewhere, indicative of snow; radial pattern in northern sector is due to low-level blockage of the radar beam by nearby towers and trees.

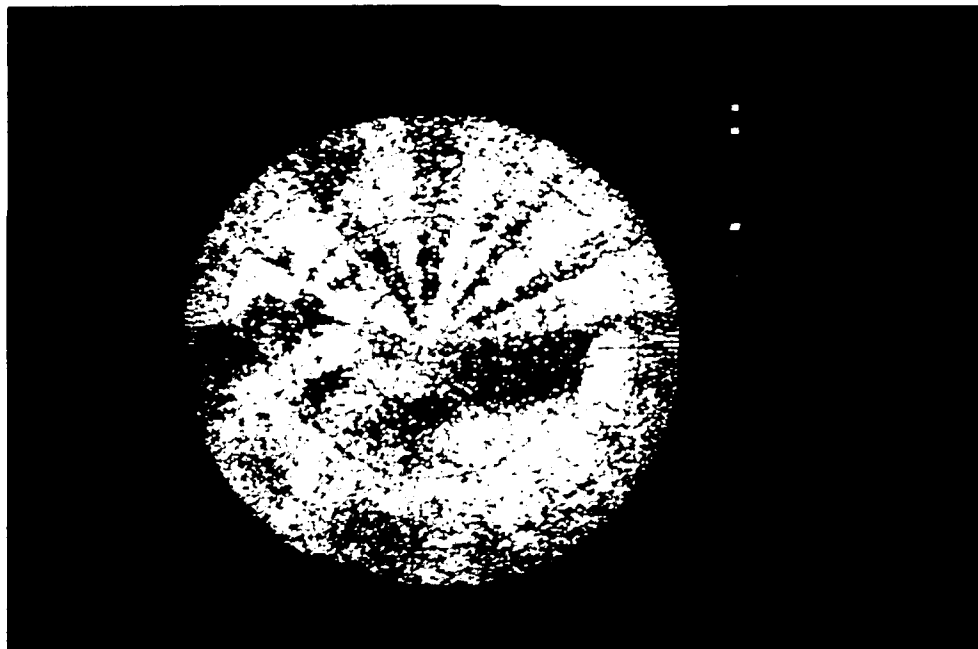
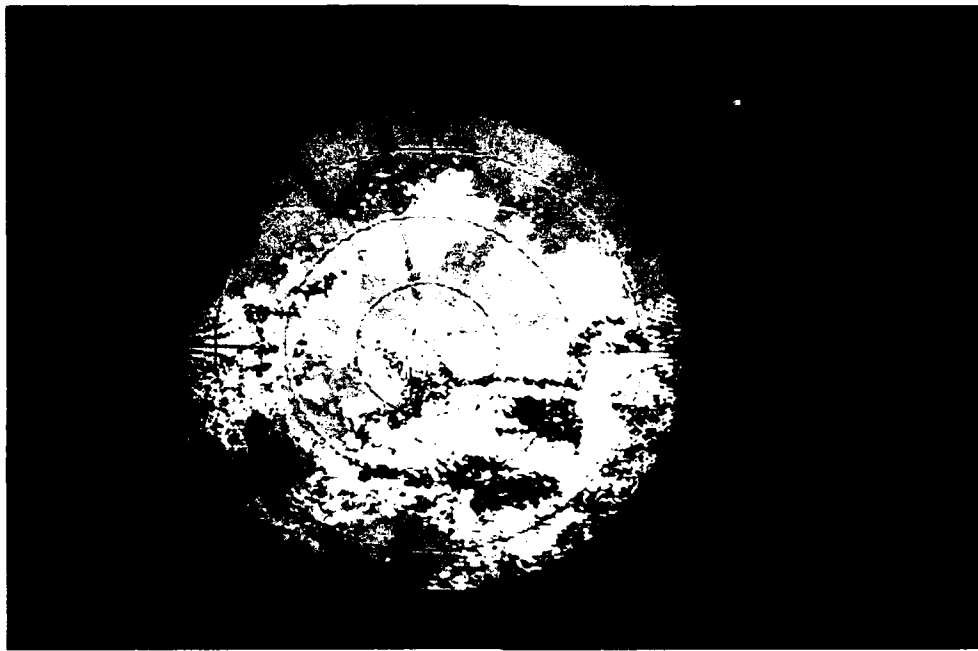


Figure 6. Absolute and Differential Reflectivity at 1021 EST. Azimuthal scan at 0.5° elevation angle shows structure similar to that in Figure 5, except that regions of high absolute reflectivity (*upper panel*) and positive differential reflectivity (*lower panel*) have moved northward to ranges of 25 and 40 km, respectively.

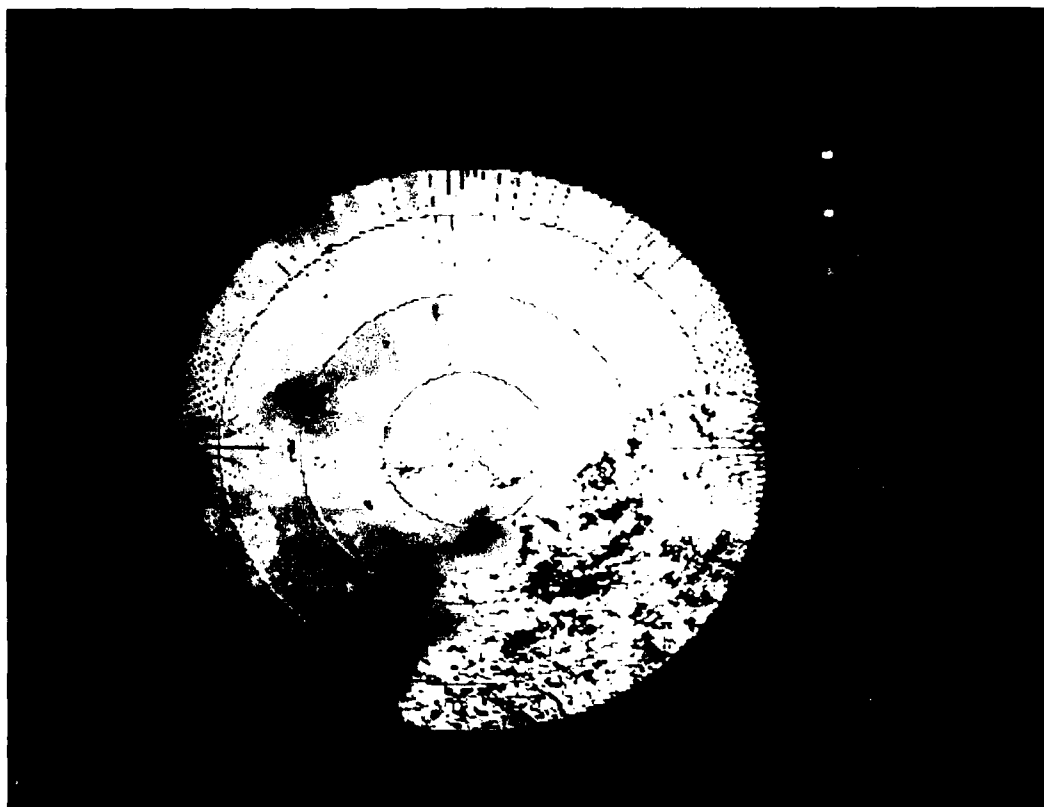


Figure 7. Absolute Reflectivity at 1112 EST. Azimuthal scan at 0.5° elevation angle with maximum range of 115 km shows band of high reflectivity southeast of the GL radar. Clearing of precipitation from the southwest had begun by this time.

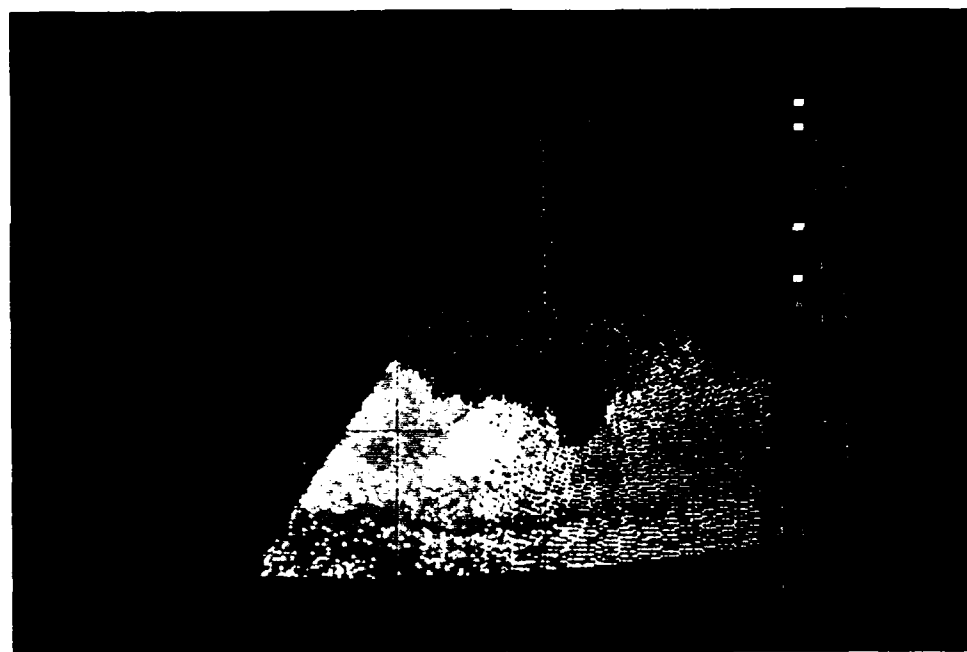
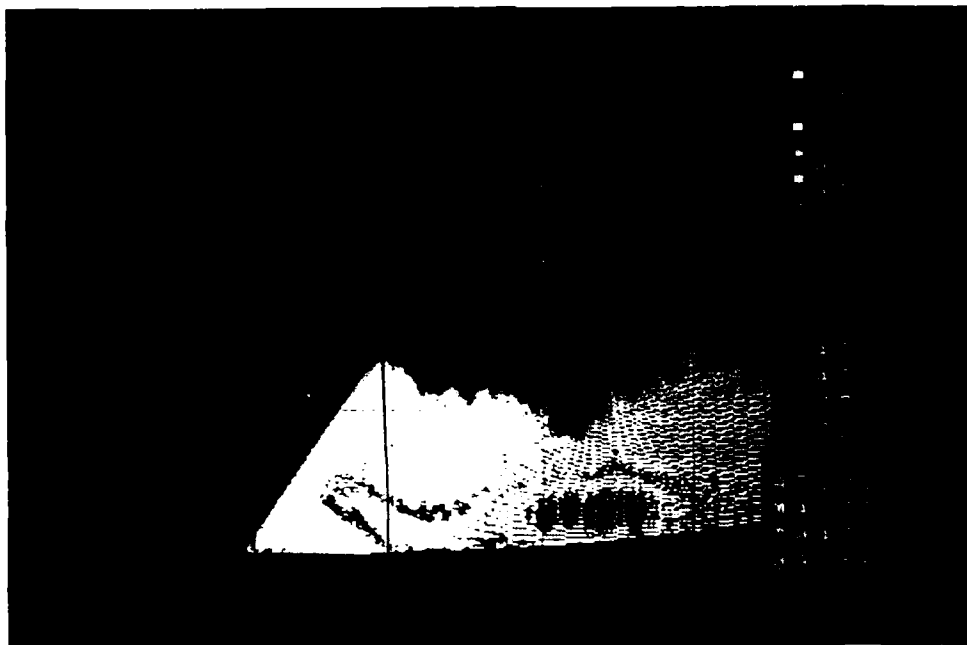


Figure 8. Vertical Section of Absolute and Differential Reflectivity at 0956 EST. Range and height are marked at increments of 32 and 4 km, respectively. Elevation angle scan at 191° azimuth shows increased absolute reflectivity (*upper panel*) and positive differential reflectivity (*lower panel*) below 2 km height and beyond 50 km range, associated with rain or mixed-phase precipitation. Region of negative differential reflectivity (green and blue) at 2–4 km height and 50–90 km range is due to detection of the low-level maximum reflectivity in a side lobe of the antenna pattern.

evolving structure of the precipitation shown on the radar display made it difficult to follow the development of the bright band in detail. The bright band gradually became better defined as it expanded azimuthally, extending through most of the southern sector by 1210 EST, when the change from snow to rain began at the GL radar site. By 1215 EST it had expanded into the northeast quadrant, dipping down to about 1 km height (Figure 9), and by 1230 EST it was detectable at all azimuths. The change of phase of precipitation in Bedford, Mass. (18 km on 69° azimuth from the GL radar), was more gradual than at Norwood, possibly because the reporting station in Bedford (at L. G. Hanscom Field) lies in a basin in which cold air can be trapped near the ground. Hourly observations from Bedford reported snow through 1200 EST, mixed snow and rain at 1300 and 1400, snow at 1500, and rain at 1700 and thereafter (the 1600 EST observation was missing). The bright band observed by the GL radar persisted near 1 km height until about 1400 EST, when the steady rain ended at the radar site. The temperature at the radar site reached 0° C about 1200 EST and increased slowly to 0.5° C by 1300 EST and 1.0° C at 1600 EST. The observations of absolute and differential reflectivity thus provide strong evidence of the advection of warm air aloft while the air near the surface remained quite cold. This is consistent with the thermal structure shown in Figures 1 and 3 and with the kinematic observations described below.

4.2. Mesoscale Wind Perturbations Aloft

The structure of the storm began to change about 1100 EST. As noted above, the precipitation structure exhibited more spatial variability after this time. Two noteworthy features appeared in the Doppler velocity displays about this time. At 1047 EST a rotational couplet of maximum and minimum Doppler velocities, separated by about 13 km, appeared near the edge of the surveillance area almost due south of the radar. Discernable first at elevation angles of 1.5 and 2.5° (about 2.7 and 4.5 km height at 102 km range), the couplet moved almost due northward at a speed of 90–100 km hr⁻¹. Figure 10 shows its position near 80 km range at 1101 EST. By 1124 EST, at 44 km range, it was discernable only at 3.5 and 4.5° elevation

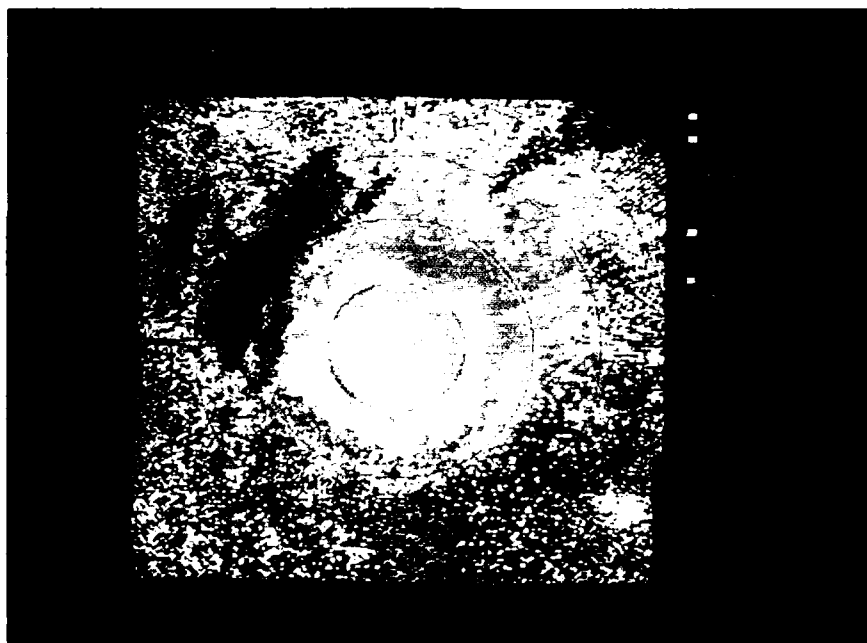


Figure 9. Absolute and Differential Reflectivity at 1219 EST. Range is marked at increments of 16 km. Azimuthal scan at 3.4° elevation angle shows "bright band" in absolute reflectivity (*upper panel*) at 16–24 km range (1.0–1.5 km height) and in differential reflectivity (*lower panel*) at 13–19 km range (0.8–1.2 km height), extending approximately from northeast clockwise through southwest and sloping upward toward the south. Change of precipitation from snow to mixed phase occurred at the radar site about this time.

(2.7 and 3.5 km height). The minimum and maximum velocities remained nearly constant, about -35 and -20 m sec⁻¹, respectively. The average of these is -99 km hr⁻¹, which is approximately equal to both the forward speed of the couplet and the wind speed at 2–4 km height derived from the analysis of dual Doppler radar measurements. This velocity couplet thus was strongly suggestive of a vortex embedded in the southerly flow between 2 and 5 km height. It was associated with a slight enhancement of the reflectivity, but it did not appear to influence the velocity field below 2 km height, probably because of the strong static stability in the lowest 2 km.

While this feature was still identifiable, another maximum and minimum of the Doppler velocity appeared in the southern sector. This second feature, larger than the first, was discernible near the edge of the surveillance area, beyond 100 km range, about 1120 EST. By 1135 EST it was identifiable at the lowest three elevation angles (0.5° , 1.5° , and 2.5°) at ranges of 80–95 km. During a period of about 2.5 hr this feature moved gradually northeastward; for most of this time, the minimum of the inward Doppler velocity appeared about 30–40 km west or southwest of the maximum. By 1315 EST the maximum inward Doppler velocity was identifiable at all five elevation angles. Azimuthal displays of the Doppler velocity at elevation angles of 1.5° and 2.5° about this time are shown in Figure 11. The feature appeared only in the upwind (southern) sector of the displays; at no time did any corresponding feature appear in the downwind (northern) sector. The preliminary interpretation of this feature³ was that it was due to a mesoscale vortex. Analysis of the horizontal wind fields, discussed in more detail below, revealed that the observed Doppler velocity structure was due not to a vortex but to a mesoscale trough and ridge. With this knowledge, one can reexamine the Doppler velocity data from the GL radar and find that the observed features have more continuity in the horizontal than in the vertical and that, unlike a vortex embedded in the observed wind field, they have a significant component of motion perpendicular to the wind vector.

In an attempt to understand the velocity structure better, we synthesized the two-dimensional horizontal wind field at several heights from data acquired by the GL radar and the MIT radar. This was accomplished by means of the Doppler radar data analysis software package known as CEDRIC, which was developed at the National Center for Atmospheric

Research in Boulder, Colo.,⁹ and installed on the VAX 11/750 computer at the GL radar field site. We performed the analysis on an 80-km square grid south and southeast of the radars (see Figure 2), encompassing most of the region within which the unusual Doppler velocity features were seen. The Doppler velocity data were dealiased, interpolated to the grid with resolutions of 1 km horizontally and 0.5 km vertically (from 1 to 4 km height), and edited to remove obviously incorrect values prior to synthesis. The synthesized zonal (u) and meridional (v) components were patched to improve spatial continuity, filtered by means of the method developed by Leise,¹⁰ and used for computation of the two-dimensional divergence ($\partial u/\partial x + \partial v/\partial y$) and the vertical component of vorticity ($\partial v/\partial x - \partial u/\partial y$) in the horizontal planes. The Leise filter was applied with three "steps;" this procedure, which yields a scale size of about 8 km in the filtered data, was necessary to eliminate smaller-scale variability of the divergence and vorticity fields that was due to noisy radar data. (Some of this variability is due to blockage and reflection of the beam of the MIT radar at low elevation angles by tall buildings.)

Analyses of volume scans beginning at 1214, 1245, 1314, 1335, and 1401 EST show that the analysis area initially was dominated by a strong southerly flow at 1.5 km height and above; a region of weaker south-southwesterly flow advanced across the grid, initially at a speed of about 11 km hr⁻¹. It is the difference between these flows that appears as the couplet in the Doppler velocity displays. The horizontal vector wind fields at 2 km height at 1314 and 1401 EST are shown in Figure 12 as examples of the analytical results. The evolution of the wind field is further illustrated in Figure 13 by hodographs of the mean wind in the analysis grid. As the region of weaker flow advanced across the grid, the mean wind speed at all levels decreased. In addition, the winds at 1.5 km and above veered with time, because of the westerly component behind the advancing wind shift line. We should note that the mean values presented in Figure 13 are calculated only within the domain of signal detectable by both radars; they

Scale of *Doppler (radial) mean velocity* in Figures 10, 11, and 16 runs from -27.65 to +27.65 m sec⁻¹. Green, yellow, and red denote positive (outward) velocities; blue and magenta denote negative (inward) velocities. Color scale wraps around on itself to denote higher velocities, which are said to be "folded" or "aliased."

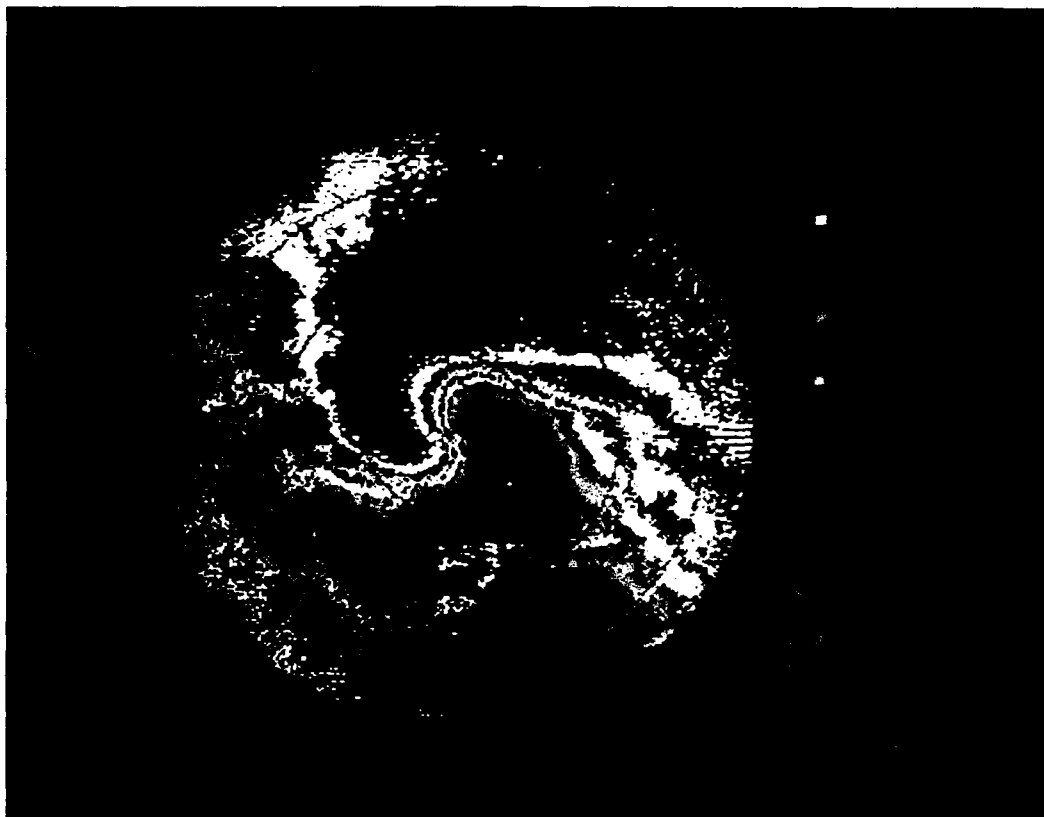


Figure 10. Doppler Mean Velocity in Azimuthal Scan at 1101 EST. Elevation angle is 2.5° , and range is marked at increments of 32 km. Color scale is described in footnote on Page 18. Wind is east-northeasterly at the surface and veers with height to southerly at 2.8 km (64 km range); maximum speed is about 40 m sec from the southeast at 1.7 km height (40 km range). Rotational couplet of maximum and minimum velocities is near 80 km range almost due south of the radar.

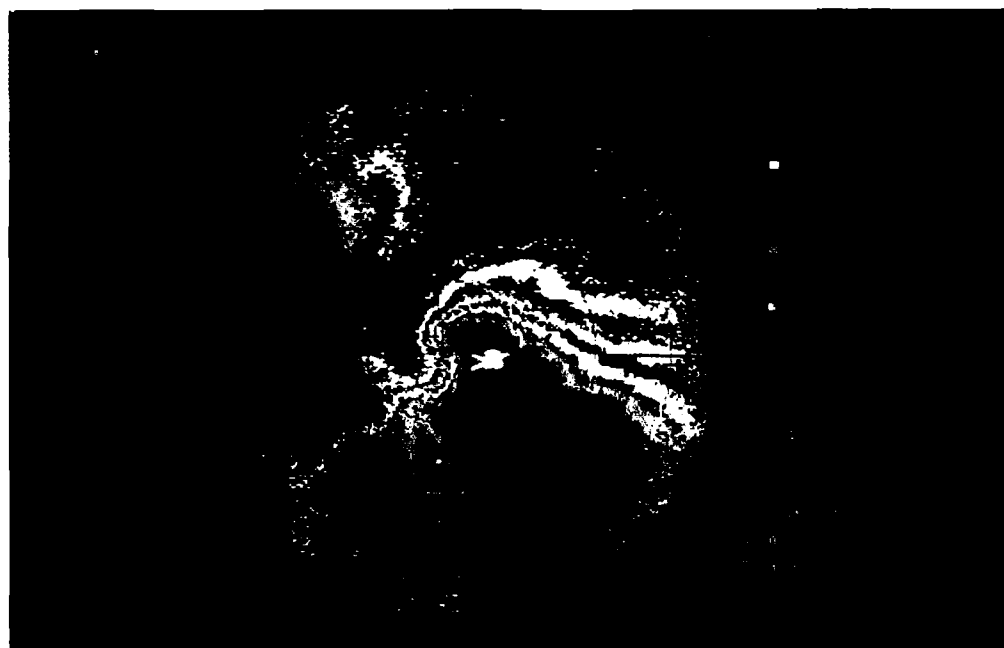
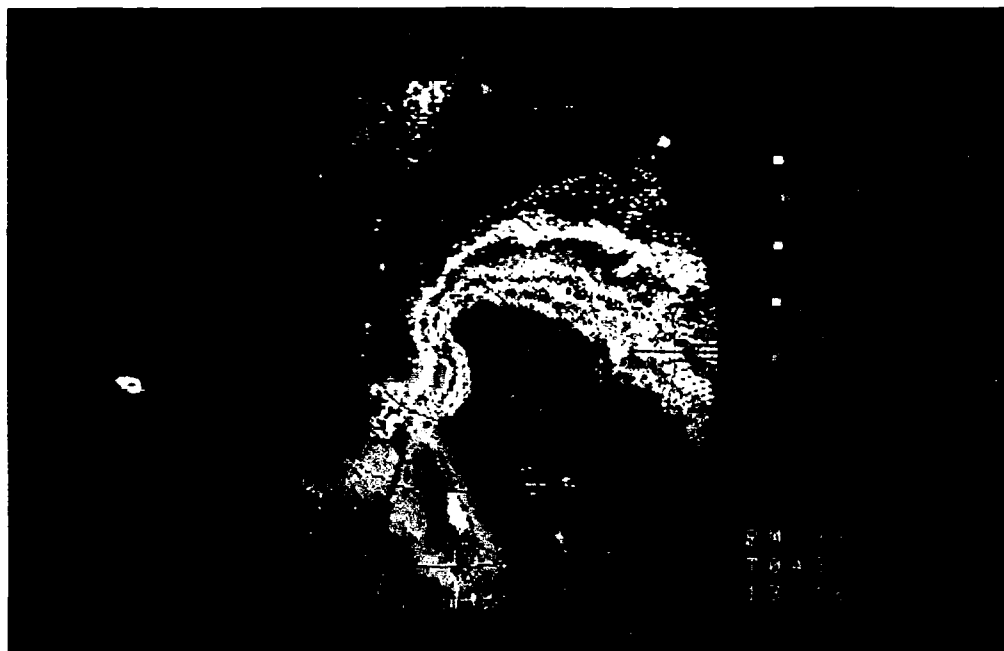


Figure 11. Doppler Mean Velocity in Azimuthal Scans at 1316 EST. Range is marked at increments of 32 km. Scans at elevation angles of 1.5° (*upper panel*) and 2.5° (*lower panel*) show increased inward (southerly) flow at ranges of 40–100 km in the southeast, just east of the advancing region of weaker southwesterly flow. Note the absence of corresponding features on the northern side of the display.

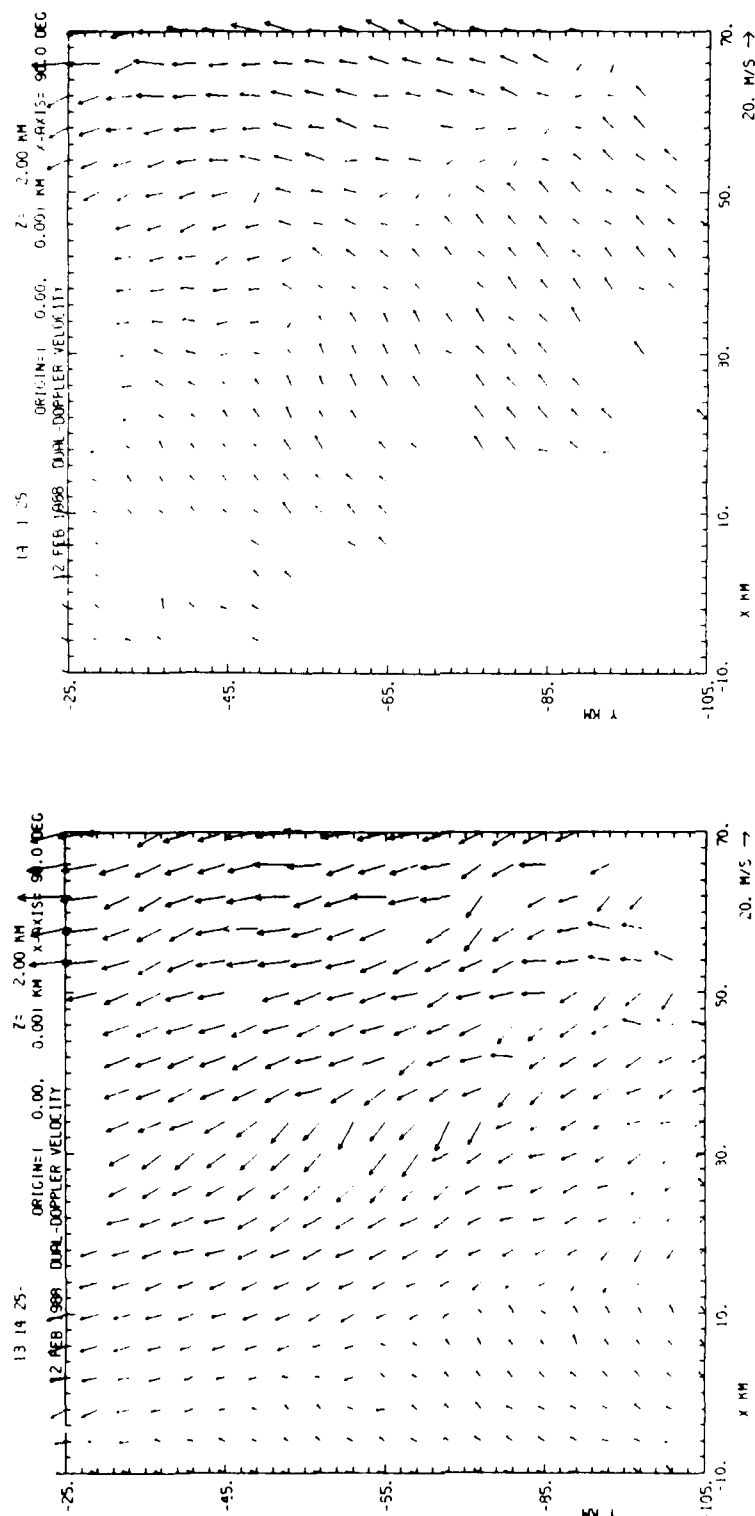


Figure 12. Synthesized Velocity Fields at 1314 and 1401 EST. Synthesis was performed on analysis grid shown in Figure 2. Coordinates are relative to the GL radar. Unfiltered velocity fields at a height of 2 km at 1314 EST (*right*) and 1401 EST (*left*) show strong southerly flow on eastern side of grid and weaker southwesterly flow advancing from the southwest. Line of wind shift extends from upper left to bottom center at 1314 EST and from top center to bottom right at 1401 EST.

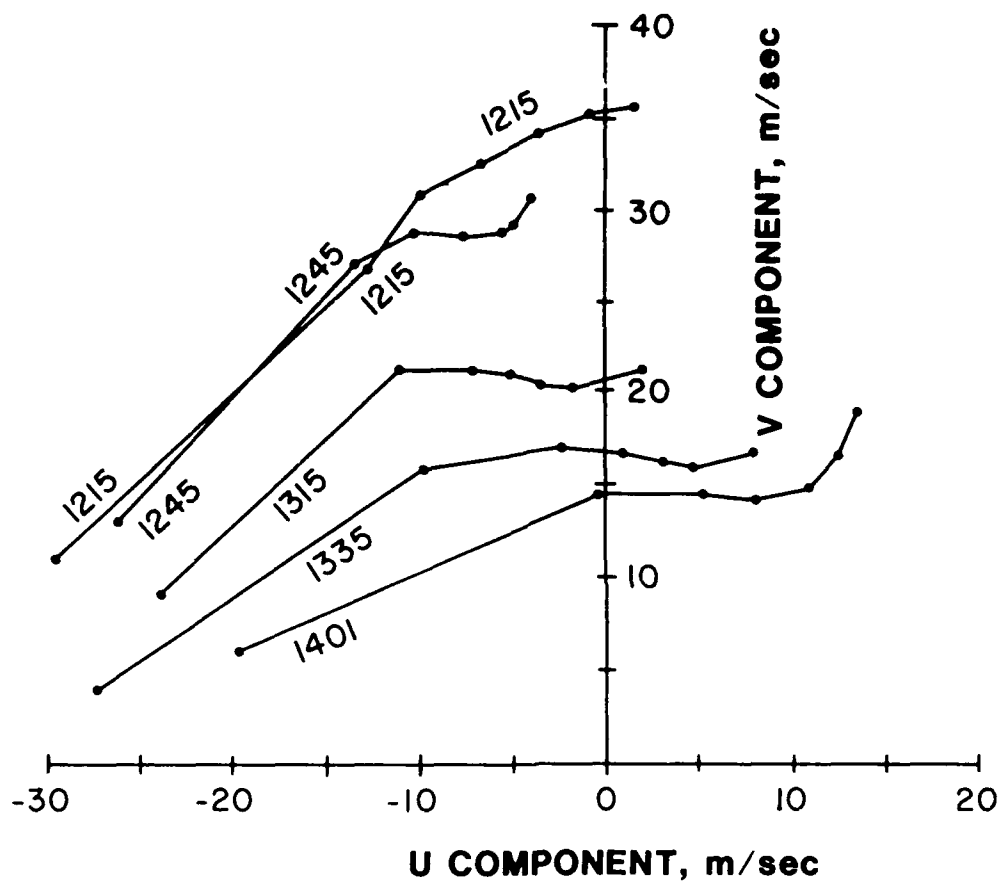


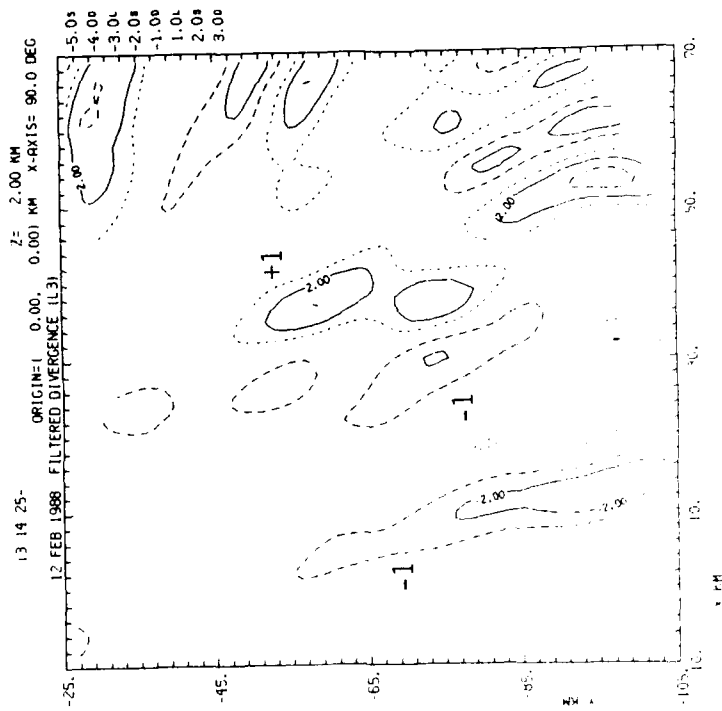
Figure 13. Profiles of Mean Horizontal Wind in Analysis Grid. Plotted points denote wind vector from 1–4 km height at intervals of 0.5 km. Wind at most heights veers with time and decreases in speed as region of weaker southwesterly flow advances across the grid.

are not true averages over the entire 80 km square grid. At 1 km height, for example, the data extend only to the range at which the MIT radar beam intersects this surface at its lowest elevation angle. Hence, Figure 13 would not reveal the effect of the advancing southwesterly flow at 1 km height, even if that flow were present there.

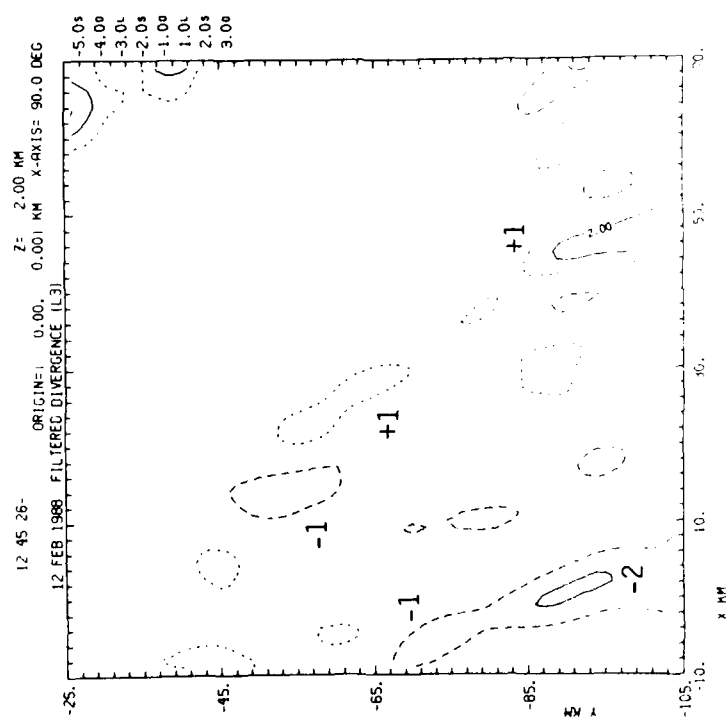
It is of interest to compare temperature gradients derived by the thermal wind equation with those derived from surface and upper air temperature data. The wind shears in the six layers between 1 and 4 km at 1214 EST yield gradients of 0.13, 0.028, 0.019, 0.019, 0.016, and 0.013 K km⁻¹. With the exception of the lowest layer, these compare well in both magnitude and direction with the observed gradients of 0.025 K km⁻¹ on the 850 mb surface at 1.5 km height (Figure 1) and 0.013 K km⁻¹ on the 700 mb surface at 3 km height. Although the strong shear between 1 and 1.5 km is inconsistent with the observed gradients aloft, we should note that the gradient at the surface below the analysis grid was 0.08–0.1 K km⁻¹, with isotherms oriented from southwest to northeast, during the time of these radar observations.

The wind shift line that is evident in Figure 12 is associated with distinct features in the fields of divergence and vorticity. At 1245 EST the wind shift line coincided with an elongated area of convergence, evident from 1.5 to 4 km height, and a similar area of positive vorticity, evident from 1.5 to 2.5 km. As shown in Figures 14 and 15, these features persisted as the line advanced across the grid, except that an area of divergence progressively developed ahead of the convergence area. Between 1335 and 1401 EST the movement of these features was greatly accelerated, relative to their speed between 1214 and 1335 EST. One might doubt their continuity in the later interval but for the obvious characteristics of the velocity field at 1401 EST (Figure 11b).

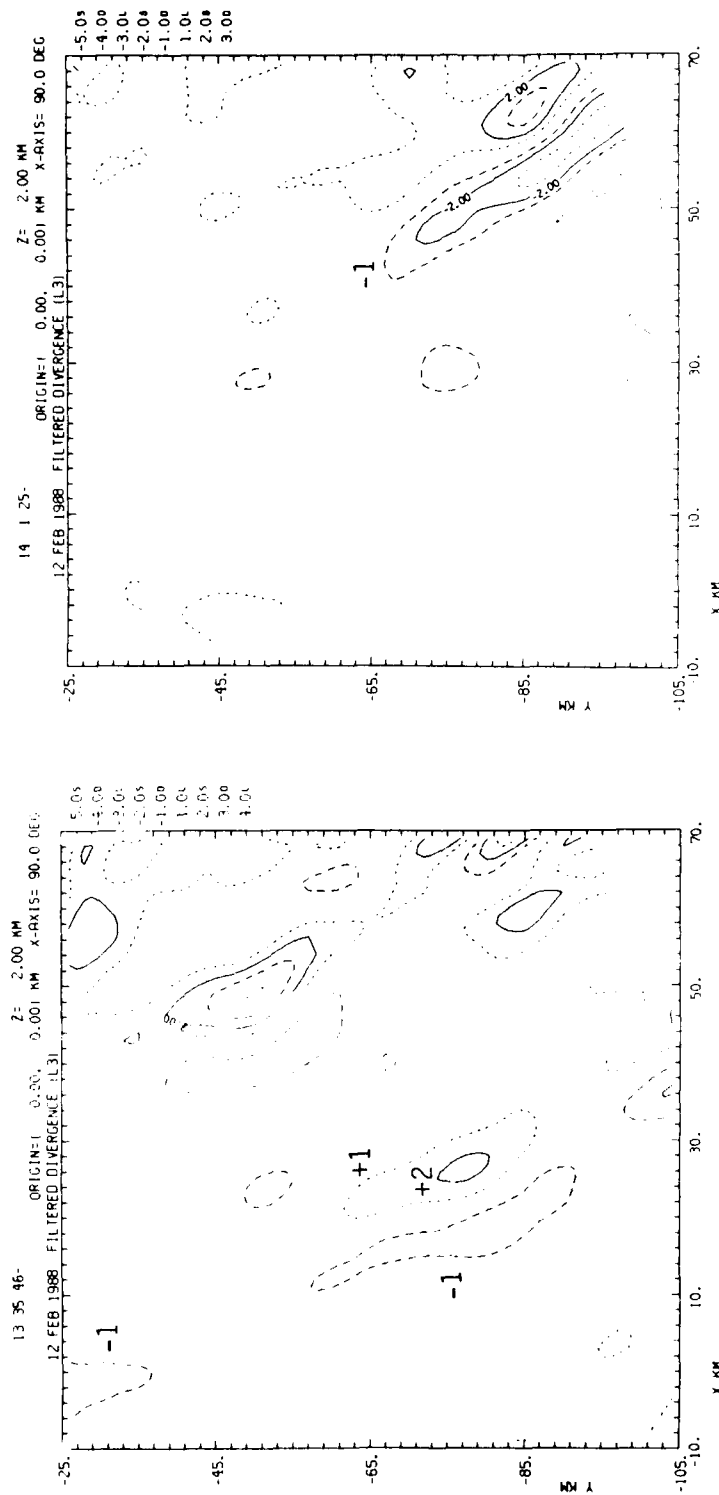
It was not possible to examine the subsequent development and movement of these features in detail, however, because of the increasing difficulty of reliable velocity synthesis to the east and southeast of the dual-radar baseline. We can, however, examine the Doppler velocity data from the GL radar to obtain some information on the subsequent developments. We find that, with the knowledge gained from the dual-Doppler analysis, we can identify the wind shift line as early as 1215 EST. It is readily



Panel b



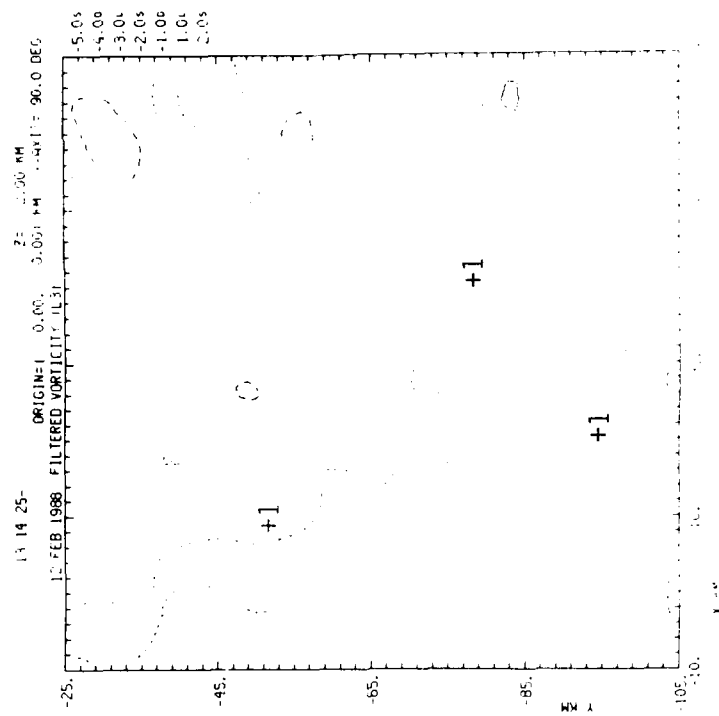
Panel a



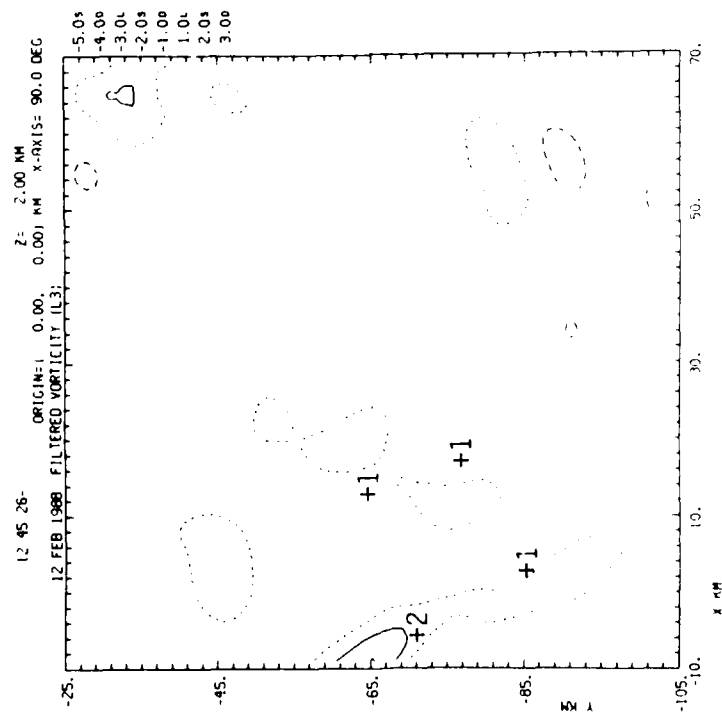
Panel c

Panel d

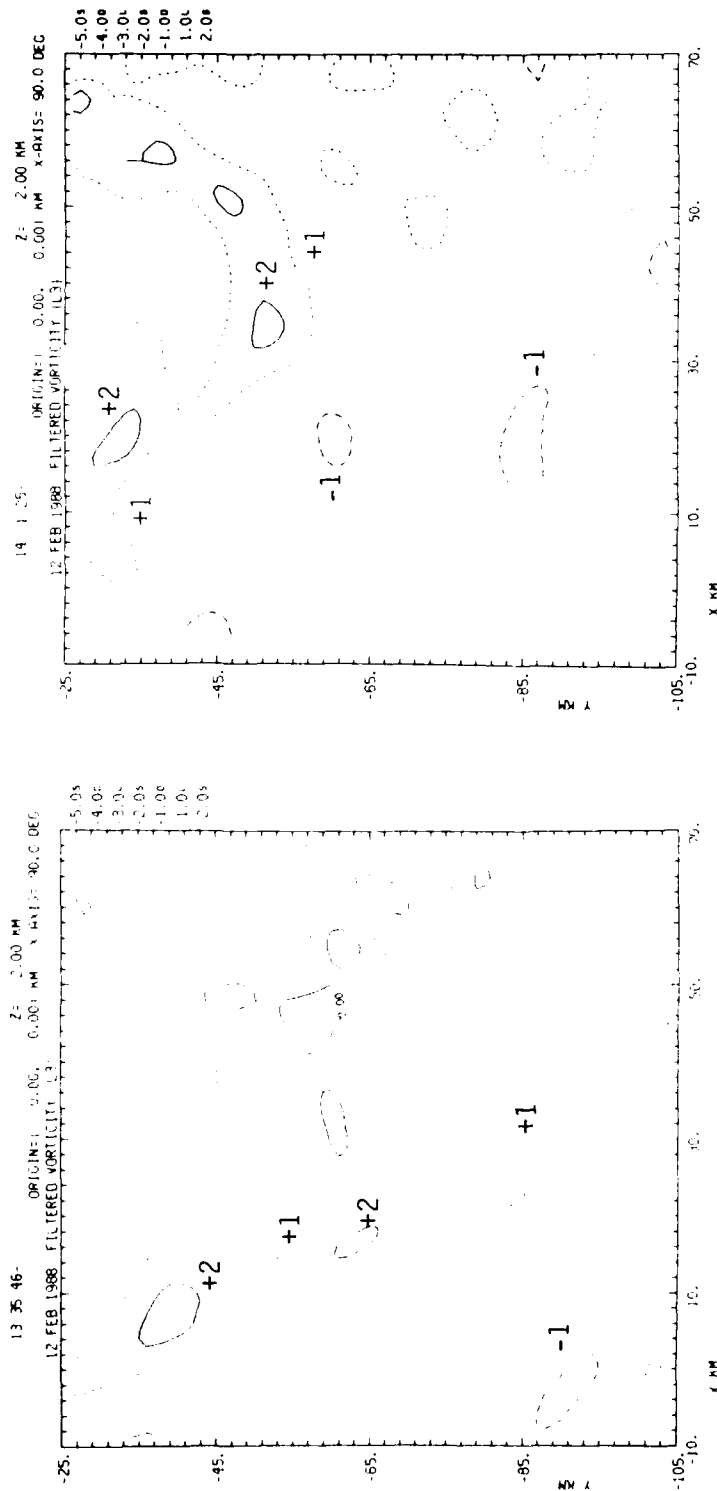
Figure 14. Horizontal Divergence at 2 km Height. Plotted quantity is $\partial u/\partial x + \partial v/\partial y$ calculated from filtered velocity components; contours denote units of 0.001 sec^{-1} between -0.005 and $+0.005 \text{ sec}^{-1}$ with the zero contour suppressed. Panels a-d correspond to 1245, 1314, 1335, and 1401 EST, respectively. Wind shift line coincides with narrow band of convergence moving across the grid. Convergence is evident at heights of 1.5-4 km. Band of divergence develops ahead of the convergence as the wind shift line advances.



Panel b



Panel a



Panel c

Panel d

Figure 15. Vertical Vorticity at 2 km Height. Plotted quantity is $\partial v / \partial x - \partial u / \partial y$ calculated from filtered velocity components; contours values are identical to those in Figure 14. Panels a-d correspond to 1245, 1314, 1335, and 1401 EST, respectively. Wind shift line coincides with band of positive vorticity, which was evident at heights of 1.5-2.5 km. Bands of positive vorticity in northeast part of grid at 1335 and 1401 may be analytical artifacts; they are approximately concentric to the MIT radar (x, y coordinates 32.7 km, -5.8 km) and may be due to erroneous velocity gradients introduced when the radar data are interpolated to the analysis grid.

evident in Figure 11, for example. The line is identifiable in the Doppler velocity displays as late as 1420 EST. The eastward movement of the wind shift line preceded the clearing of the heaviest precipitation throughout this period, which is discussed in more detail in Section 4.3 below.

Several related observations support the interpretation that a mesoscale trough and ridge of limited vertical extent moved across the analysis grid. Azimuthal displays of Doppler mean velocity indicate that the southerly component of wind at 1.5–4 km height to the south of the radar gradually increased after the passage of the wind shift line. Azimuthal displays of Doppler mean velocity at high elevation angles throughout this period indicate that the flow near the top of the radar echo was not significantly changed by the passage of the wind shift line. The radar data thus suggest that a mesoscale trough, identified with the cyclonic curvature of the wind across the wind shift line, was followed by a mesoscale ridge, both of which were part of the circulation around the synoptic scale cutoff low. The wind variations identified in the radar data apparently did not extend to the surface, as there was no significant change of winds reported hourly during the passage of the wind shift line or during the clearing of precipitation.

There is some evidence in the upper air analyses to support the foregoing interpretation. The 850 mb analysis at 0700 EST (Figure 1) indicates a significant cyclonic curvature between Washington, D. C. (Sterling, Va.), where the wind was westerly, and Wallops Island, Va., and Atlantic City, N. J., where the wind was more southerly. It was not possible to track the subsequent development of this feature, however, because analyses from the National Meteorological Center were not available for 0000 and 1200 UT on 13 February. Another possibility is that the 850 mb low is in a mature stage of development and a new 850 mb low center is forming to the east, near the junction of the cold, warm, and occluded fronts. In the absence of subsequent upper air analyses, this cannot be confirmed.

4.3. Surface Weather Events

Several features of the meteorological observations at the surface are pertinent to the interpretation of the mesoscale wind fields derived from the

radar data. Throughout the day over southern New England the surface pressure fell at a rate of $1\text{--}2\text{ mb hr}^{-1}$. The hourly reports of aircraft altimeter setting reveal an area of pressure falls exceeding 3 mb hr^{-1} (0.1 inch Hg per hr) that was first observed between 0900 and 1000 EST extending across Connecticut from the north central part of the state to the southeast corner and offshore. This area of more rapidly falling pressure moved northeastward at about 40 km hr^{-1} during the following 6 hr. Its passage over the GL radar site coincided with a pressure fall of 5.5 mb between 1340 and 1415 EST (9.4 mb hr^{-1}), which was followed by a rise of 2.4 mb in 30 minutes before the pressure continued to fall at its earlier rate. Between 1340 and 1430 EST the wind at the radar site, from an azimuth of 60° , increased from an average of about 6 m sec^{-1} to about 11 m sec^{-1} , with a peak gust of 22 m sec^{-1} , and decreased to its previous value with no change of direction. These observations, particularly the pressure record, further support the hypothesis of a mesoscale trough and ridge aloft.

The early stages of development of the precipitation field were described in Section 4.1. The change of the wind field described in Section 4.2 occurred just ahead of a line of nearly complete clearing of precipitation. Within the analysis grid to the south of the GL radar the western edge of the precipitation area detected by the radar moved eastward at about 60 km hr^{-1} , initially about 50 km behind the wind shift line. To the north of the radar the western edge of the precipitation area moved eastward more slowly, about 30 km hr^{-1} between 1315 and 1420 EST, and it became almost stationary for at least 30 minutes thereafter. After 1400 EST, when the reflectivity was generally less than 7 dBZ throughout the display, a narrow ($6\text{--}10\text{ km}$ wide) band of higher reflectivity developed along the western edge of the precipitation area to the north of the GL radar. This band extended north-northeastward from the radar to about 95 km range at 1419 EST (Figure 16), with a maximum reflectivity of about 35 dBZ , and remained nearly stationary while gradually weakening during the ensuing half hour. We did not attempt to analyze the wind fields in the vicinity of this feature, as the displays of Doppler mean velocity did not exhibit any significant spatial structure or temporal variations.

These observations and analysis reveal significant details of the evolution of the storm and ultimately raise a variety of questions about the dynamics, the answers to which are beyond the scope of this report. For example, how

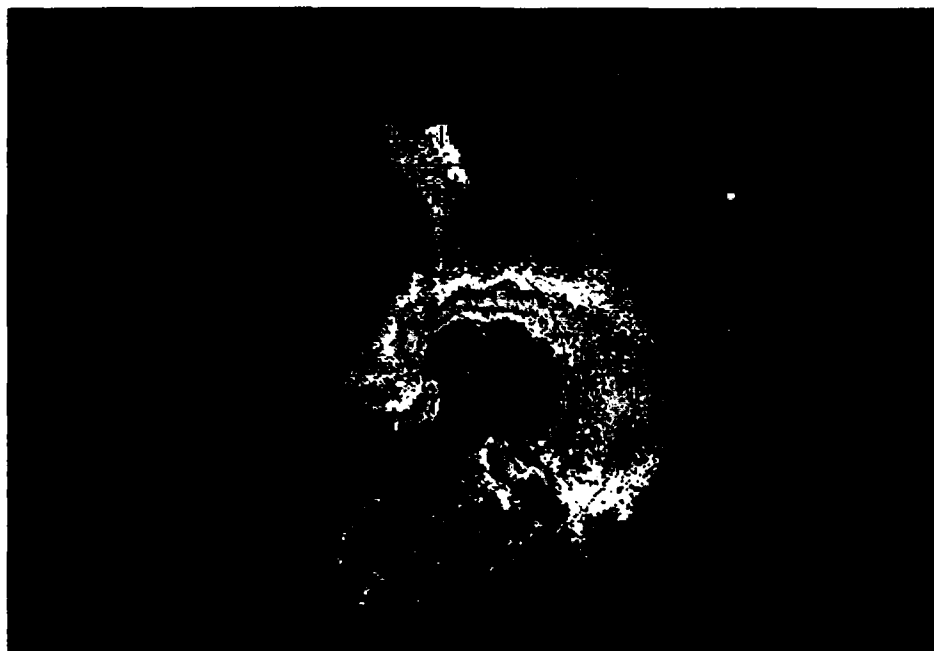
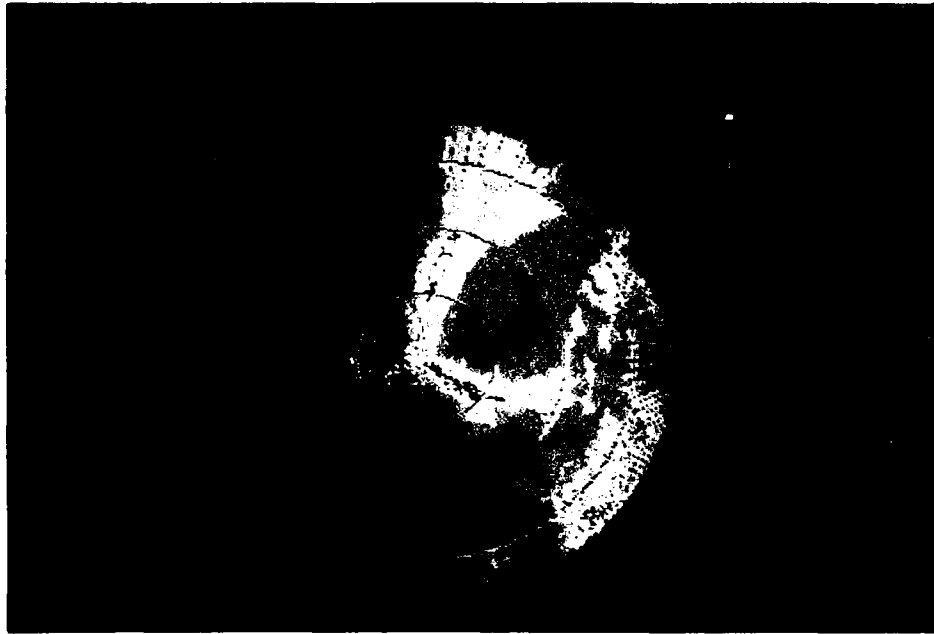


Figure 16. Absolute Reflectivity and Doppler Mean Velocity in Azimuthal Scans at 1419 EST. Narrow bands of enhanced absolute reflectivity shown at 0.5° elevation (*upper panel*) are probably due to localized convergence associated with the mesoscale trough. Region of weak southwesterly flow is shown by positive Doppler velocity (green) centered at 64 km range to the southeast at 1.5° elevation angle (*lower panel*).

is the mesoscale trough and the intrusion of drier air related to the movement and intensification of the surface low pressure center to the south? It seems likely that the mesoscale trough and ridge were responsible for the fact that nearly all the precipitation occurred well in advance of the surface low pressure center. Where does the dry air originate? The 850 mb analysis at 0700 EST (Figure 1) indicates drier air over stations to the southwest. The Chatham sounding (Figure 3) indicates drier air between 850 and 700 mb, which may have subsided within the mesoscale ridge. A more precise understanding of these phenomena is essential to the development of improved quantitative precipitation forecasting techniques.

5. SUMMARY

We have described mesoscale features of a coastal storm that occurred on 12 February 1988. Of particular interest are the apparent relationship of the differential reflectivity to the northward progression of the rain/snow line and the evidence of warm air advection aloft near the radar site. It is also of interest that the "bright band" was not well defined in either the absolute reflectivity or the differential reflectivity when the rain was beyond 35 km range from the radar but that a distinct bright band in both quantities appeared above the radar site coincident with the transition to rain. These characteristics were associated with strong static stability and the advection of warm air in the lowest 2 km of the atmosphere. In the later stages of the storm, there was an intrusion of drier air at 1.5–4 km height in association with a mesoscale trough and ridge. There was an increasing southerly flow at these heights ahead of an advancing wind shift line, with weaker southwesterly flow in the drier air behind. The difference of these flows gave the appearance of a mesoscale vortex in azimuthal displays of the Doppler mean velocity. The mesoscale trough closely preceded the large-scale clearing of precipitation from the west, which occurred well in advance of the passage of the low pressure center to the south.

Although the analysis reported here relies on dual Doppler radar wind measurements, the results are applicable to observations of extratropical storms by single Doppler radars. The Doppler velocity data provide

information about the upper air circulation that is not generally derivable from analyses at the synoptic scale, because of the limited spatial and temporal resolution of the upper air data. The mesoscale trough and ridge that we deduced from our analysis produced distinct features in the displays of Doppler velocity and evidently had a significant impact on the development of the precipitation.

The analysis reported here is the first use of the dual-Doppler radar capability provided by the 11-cm radars at GL and MIT. We contemplate the continued use of these facilities in the future for investigations of storm dynamics and microphysics, with increasing emphasis on the expanded polarimetric capabilities of the GL radar.

References

1. Bishop, A. W., and Armstrong, G. M. (1982) *A 10 cm Dual Frequency Doppler Weather Radar, Part I: The Radar System*, AFGL-TR-82-0321(I), AD A125885.
2. Ussailis, J. S., Leiker, L. A., Goodman, R. M., IV, and Metcalf, J. I. (1982) *Analysis of a Polarization Diversity Weather Radar Design*, AFGL-TR-82-0234, AD A121666.
3. Ruggiero, F. H., and Donaldson, P. J., Jr. (1989) Features resembling single-Doppler vortex signatures observed in an extratropical cyclone, *Preprints 24th Conf. Radar Meteorol.* (Tallahassee), Amer. Meteorol. Soc., Boston, 249–243.
4. Stewart, R. E. (1984) Deep 0° C isothermal layers within precipitation bands over southern Ontario, *J. Geophys. Res.*, **89**, 2567–2572.
5. Szeto, K. K., Stewart, R. E., and Lin, C. A. (1988) Mesoscale circulations forced by melting snow. Part II: Application to meteorological features, *J. Atmos. Sci.*, **45**, 1642–1650.
6. Bosart, L. F., Vaudo, C. J., and Helsdon, J. H., Jr. (1972) Coastal frontogenesis, *J. Appl. Meteorol.*, **11**, 1236–1258.
7. Seliga, T. A., and Bringi, V. N. (1976) Potential use of radar

- differential reflectivity measurements at orthogonal polarizations for measuring precipitation, *J. Appl. Meteorol.*, **15**, 69–76.
8. Metcalf, J. I., panel leader (1990) Technology of polarization diversity radars for meteorology: Panel report, *Radar in Meteorology* (D. Atlas, ed.), Amer. Meteorol. Soc., Boston, Chap. 19b, 191-198.
 9. Mohr, C. G., and Miller, L. J. (1983) CEDRIC—A software package for Cartesian space editing, synthesis, and display of radar fields under interactive control, *Preprints 21st Conf. Radar Meteorol.* (Edmonton), Amer. Meteorol. Soc., Boston, 569–574.
 10. Leise, J. A. (1981) *A Multidimensional Scale telescoped Filter and Data Extension Package*, NOAA Tech. Memo. ERL/WPL-82, Wave Propagation Laboratory, Natl. Oceanic and Atmos. Admin., Boulder, Colo., 20 pp.